Max-Planck-Institut
für Mathematik
in den Naturwissenschaften
Leipzig

A single cell based-model of tumor growth in-vitro: monolayers and speroids

by

Dirk Drasdo and Stefan Höhme

Preprint no.: 58 2005

A single cell based-model of tumor growth in-vitro: monolayers and spheroids

Dirk Drasdo†§ and Stefan Höhme‡

† Interdisciplinary Centre for Bioinformatics, University of Leipzig, Härtelstr. 16-18, D-04107 Leipzig, Germany, and
Max-Planck-Institute for Mathematics in the Sciences, Inselstr. 22-26, D-04103 Leipzig, Germany
‡ Interdisciplinary Centre for Bioinformatics, University of Leipzig, Härtelstr. 16-18, D-04107 Leipzig, Germany

Abstract. To what extent the growth dynamics of tumors is controlled by nutrients, biomechanical forces, and other factors at different stages and in different environments is still largely unknown. Here we present a biophysical model to study the spatio-temporal growth dynamics of two-dimensional tumor monolayers and three-dimensional tumor spheroids as a complementary tool to *in-vitro* experiments. Within our model each cell is represented as an individual object and parameterized by cell-biophysical and cell-kinetic parameters that can all be experimentally determined. Hence our modeling strategy allows to study which mechanisms on the microscopic level of individual cells may affect the macroscopic properties of a growing tumor. We find the qualitative growth kinetics and patterns in early growth stages to be remarkably robust. Quantitative comparisons between computer simulations using our model and published experimental observations on monolayer cultures suggest a biomechanically-mediated form of growth inhibition during the experimentally observed transition from exponential to sub-exponential growth at sufficiently large tumor sizes. Our simulations show that the same transition during the growth of avascular tumor spheroids can be explained largely by the same mechanism. Glucose (or oxygen) depletion seems to determine mainly the size of the necrotic core but not the size of the tumor. We explore the consequences of the suggested biomechanical form of contact inhibition, in order to permit an experimental test of our model. Based on our findings we propose a phenomenological growth law in early expansion phases in which specific biological small-scale processes are subsumed in a small number of effective parameters.

PACS numbers: 87.18.-h, 87.

§ To whom correspondence should be addressed (drasdo@izbi.uni-leipzig.de)

1. Introduction

Despite extensive experimental studies it is still not fully understood which factors determine the growth kinetics and spatial structure of tumors in different growth stages both, in-vivo and in-vitro. A comprehensive understanding of this issue may be facilitated combining in-vivo observations (Hart et al., 1998, Swanson et al., 2000, Schiffer et al., 2003); experiments in-vitro, in which well-defined growth conditions can be established (Santini and Rainaldi, 1999, Mueller-Klieser, 2000); and mathematical modeling, where hypotheses can be tested free from uncontrolled or unknown experimental influences (Marusic et al., 1994, Chaplain, 1996, Ward and King, 1997, Jones et al., 2000, Byrne et al., 2001, Chen et al., 2001, Moreira and Deutsch, 2002, Byrne and Prezziosi, 2003).

Bru et al. (1998) have grown two-dimensional tumor monolayers from C6 rat astrocyte glioma cells. They observed a linear growth of the tumor (monolayer) diameter L with time t (Fig. 1c). Thus even though all cells were in contact with the nutrient medium, the growth was linear rather than exponential. This suggests that the division of non-boundary cells is repressed by a form of contact inhibition. Freyer and Sutherland (1985, 1986) investigated the effect of glucose and oxygen on spheroid growth of EMT6/Ro mouse mammary carcinoma cell spheroids. During the first 3-4 days, the number of cells N increased exponentially. After 4 days, N increased only sub-exponentially accompanied by a linear growth of the tumor spheroid diameter L (Fig. 1c). Guided by the Gompertz growth law, which is characterized by exponential growth in early stages and saturation at later stages, Freyer and Sutherland (Freyer and Sutherland, 1985) concluded that the sub-exponential regime of N indicates saturation. In reanalyzing that data we found that as long as the glucose and oxygen medium concentrations were not too small, a plot of $N^{1/3}$ vs. time t (Fig. 1a) indicates a power-law-like behavior $N \propto t^{\eta}$ with $\eta \approx 3$ rather than a saturation. This indicates that curve fitting by purely phenomenological, macroscopic growth models such as the Gompertz model can be misleading, if the models do not properly reflect the mechanisms responsible for determining the shape of the growth curve. The findings reported above have stimulated us to compare the growth of tumor monolayers and spheroids within the framework of a single-cell based mathematical model, with emphasis on the role of the nutrient supply, biomechanical forces on individual cells and kinetic cell properties. In addition to phenomenological, macroscopic growth laws (Marusic et al., 1994) a number of models of tumor growth have been considered to date. These can divided into (i) single-cell based models, including cellular automaton models (e.g. Moreira and Deutsch (2002), Alber et al. (2002), and refs. therein), and off-lattice models (e.g. Drasdo (2003) and refs. therein), and (ii) continuum models. Cellular automata (CA) represent a fictitious oversimplified micro-world (Rivet and Boon, 2001) and are based on a set of rules on a lattice which nevertheless can show a remarkable correspondence to real systems on mesoscopic length scales $\gg$ cell diameter. However, effects such as cell size changes, and mechanical deformations or compressions of cells or of cell aggregates are hard to

represent by a CA. Moreover, recent measurements show that the elastic modulus of cancer cells is often smaller than the elastic modulus of normal cells (Guck et al., 2005), and may therefore be an important model parameter. Off-lattice models can deal with such situations more easily. Continuum models include those models that represent a tumor as an elastic continuum (e.g. Jones et al. (2000)), a fluid (e.g. Byrne et al. (2001)), or kinetic equations such as the Fisher-KPP equation (e.g. Swanson et al. (2000)) i.e., the logistic equation extended by a diffusion term. The Fisher-KPP equation predicts that the cell population size initially grows exponentially, and crosses over to a linear expansion of the population diameter at advanced stages. The exponential growth of the population size is accompanied by an expansion of the diameter according to $L \propto \sqrt{t}$, which we believe is not appropriate for compact tumors in the initial growth phase. Most of the continuum approaches are deterministic and are able neither to cover the correct system behavior if stochastic fluctuations become important, nor to detect information that is reflected only in stochastic fluctuations.

Although our model does not reproduce every minute detail of cells and cell populations, we hope to illustrate that a model parameterized by characteristic, measurable properties of cells and their environment is capable of explaining many growth characteristics of in-vitro tumors. Our model may be viewed as a step towards a counterpart of molecular models in fluid dynamics, and may guide the development of other model types (here an individual molecule corresponds to an individual cell). To illustrate this, we propose a phenomenological growth law derived from our single-cell based model.

Although not demonstrated in this article, the model framework presented here also permits the inclusion of an explicit representation of the intra-cellular regulatory machinery, in order to link molecular targets to coarse-grained model parameters on the cellular level. This provides a potential link between the molecular information on the sub-cellular scale and a multi-cellular phenotype.

The paper is organized as follows: In the next section (section 2), we present a mainly qualitative description of the single-cell-based model. The mathematical details have been included in the appendices. Section 3.1 presents simulation results with the single-cell-based model, while in section 3.2 a phenomenological growth law is introduced and compared to simulation results with the single-cell-based model. A summary is provided in section 4. In addition to the mathematical description of the single-cell based model in appendices A and B, appendix C contains a table with the biological and physical model parameters and explains how these model parameters were related to "technical" parameters of the model such as step sizes etc..

2. The Model

The basic units in our model are individual cells. Our model approaches each cell as an elastic, sticky particle of limited compressibility and deformability, which is capable of active migration, growth and division. Each model parameter can in principle be

experimentally determined.
The major model features and assumptions are summarized below (for details, see appendices A-C):
(I) Since isolated cells in cultures or suspensions often have a spherical shape we assume each model cell to be spherical directly after cell division (in agreement with the observations by Bru (Bru, priv. comm.)) and to deform into a dumb-bell during mitosis. We considered two variants: Within the cell cycle (i) the cell volume doubles (Fig. 2a) or (ii) increases by a factor of 1.9, (i.e. the daughter cells are smaller than their mother cell). This provides a simple way of taking into account the 2-fold decrease of the median cell volume with increasing tumor diameter over the experimental observation period (see Freyer and Sutherland (1985)). Although this decrease may be partly cycle-phase based, this is unlikely to be the sole factor for the observed 2-fold volume decrease. We would like to emphasize that the cause for the decrease of the median cell volume is not important for the conclusions in this paper.
(II) Cells in contact can form adhesive bonds (Santini et al., 1999, Chesla et al., 1998). With decreasing distance between cell centers (e.g., upon compression) the contact area between them increases. This in turn increases the number of adhesive bonds, resulting in an increasing attractive interaction. On the other hand, if cells in isolation are spherical, an increasing contact area is accompanied by an increasing deformation which results in a repulsive interaction. Furthermore cells under physiological conditions have only a moderate compressibility (Alcaraz et al., 2003). We model the combination of attractive and repulsive interactions by an interaction energy V_{ij} due to the JKR model (Carpick et al., 1999), shown in Figs. 2b, B2 (for further explanations see Appendix B).
(III) In the absence of chemotactic signals, isolated cells in suspension or culture medium have been observed to perform a random walk-like movement (Schienbein et al., 1994, Mombach and Glazier, 1996) that we characterize by the cell diffusion constant D. More mobile cells are assumed to have a larger D.
(IV) While in mechanical contact with other cells, proliferating cells exert a pressure on their neighbors. The neighboring cells try to escape this pressure by moving against the friction caused by the other neighbor cells and extracellular material (e.g. extracellular matrix) (Rosen and Misfeldt, 1980). The movement could be partly passive, due to pushing, or active, if cells migrate into the direction into which they escape the mechanical stimulus. In both cases the migration dynamics can be modeled as a friction-dominated overdamped motion. We use the standard Metropolis algorithm (Metropolis et al., 1953, Drasdo et al., 1995) to simulate a friction-dominated stochastic dynamics driven by physical interactions. According to the Metropolis algorithm a cell translation or orientation change takes place with a rate $\propto min\{1, exp[-(\sum_{i<j}(V_{ij}(t+\Delta t) - V_{ij}(t))/F_T]\}$ where t is time, Δt a time step, and F_T is a reference energy analogous to the thermal energy k_BT in fluids or gases (T: temperature, k_B:Boltzmann const.) (Beysens et al., 2000). Note that F_T here is not a consequence of collisions between cells and fluid particles but reflects the ability of a cell to actively explore its environment in a random movement (Schienbein et al., 1994,

Mombach and Glazier, 1996). The use of this simulation method is motivated by the observation that, following each growth step, all cells move to relax the configuration at least into a local equilibrium (Drasdo et al., 1995). If growth is repressed the cell population relaxes stress and expands slightly (see Fig. 4 below). A similar energy minimization concept has been proved useful to explain the sorting of embryonic cells by differential adhesion (Seinberg, 1963, Pfeiffer, 1998).

(V) Multicellular spheroids were found to be similar to avascular tumors nodules or microregions of solid tumors in terms of the kinetics of proliferating, quiescent, and necrotic cells. Motivated by the observations in Ref. (Freyer and Sutherland, 1986) (shown in Fig. 1a) for EMT6/Ro tumor spheroids, we here consider glucose to be the limiting nutrient for our model on tumor spheroids in suspension. Accordingly we assume that cells can only proliferate if the local glucose concentration $c(\underline{r},t)$ exceeds a certain threshold c_Q^{th}, and die by "necrosis" below a second threshold $c(\underline{r},t) < c_{nec}^{th} \leq c_Q^{th}$. However, the extend to which a single factor, such as a lack of nutrients, hypoxia, accumulation of waste products, or an interplay of many different factors is responsible for the limitation of growth of spheroidal tumors, is likely to depend on the particular cell type and the cultivation conditions (Casciari et al., 1992, Mueller-Klieser, 2000). For our model simulations of tumor spheroids we study situations in which a fixed glucose concentration c_0 is maintained outside the tumor, although the same results are obtained for regular refilling with only minor parameter modifications. The glucose is locally consumed by each cell with a consumption rate $\hat{\gamma}$ and can diffuse with a rate D_{gluc} (Casciari et al., 1992) The reaction-diffusion kinetics of local concentration of glucose $c(\underline{r},t)$ is modeled by

$$\partial c(\underline{r},t)/\partial t = D_{gluc} \sum_{i=1}^{d} (\partial^2 c(\underline{r},t))/(\partial r_i^2) - \hat{\gamma}\hat{\Theta}(c) n(\underline{r},t). \qquad (1)$$

Here $\hat{\Theta}(c) = 1$ if $c \geq 0$ and is zero otherwise. In our computer simulation, we solve the equation on a regular square grid where $n(\underline{r},t) \to n_{\underline{i}}$, with $n_{\underline{i}}$ being the number of cells in square $\underline{i} = (i_x, i_y, i_z)$. For our monolayer models it is not necessary to model glucose or oxygen explicitly, since in the cultured monolayer experiments by Bru et. al. (Bru et al., 1998, 2003) nutrients are equally accessible to all cells.

Multi-cellular spheroids may contain an extensive extracellular matrix (ECM) that differs in the relative amount and assembly from the corresponding monolayer cultures, and possess a three-dimensional network of cell-to-cell and cell-to-matrix interactions with an architecture and function very similar to that in-vivo (Kunz-Schughart, 1999). Here, we do not model the extracellular matrix and the potential influence of the extracellular matrix on cell migration and division explicitly, but rather focus on an expansion dynamics that is largely driven by cell-cell interactions. The properties of the substrate and the ECM are mainly subsumed in the diffusion constant and in F_T (see model assumption III and appendix A).

(VI) We assume an average intrinsic cell cycle time to be influenced at the level of individual cells by nutrients, regulatory factors and mechanical stress. We denote

τ as the average intrinsic cell cycle time of an isolated cell not affected by physical interactions with neighboring cells. In our model, a cell within a multicellular aggregate can grow only if it is not extensively deformed (or compressed). That is, if the central displacement of the surface of cell i at the contact point to its neighbor cell j does not become smaller than a critical "deformation threshold" of $(1-\zeta)l_i$ with $0 < \zeta \leq 1$ such that $d_{ij} > \zeta(l_i - l_j)/2$, see Fig. 2b and appendices B,C. I.e., we assume that cell growth can be controlled by the cells' degree of deformation, which may be sensed by the cell cytoskeleton (Huang and Ingber, 1999). (For a critical compression the line of argument is equivalent.) Consequently the observed cell cycle time of deformed cells is typically larger than the intrinsic cycle time (see Fig. 6 below). We study three cases. (i) A cell that was subject to a critical deformation continues growing as long as the deformation remains below the critical threshold, independently of how long the critical deformation has lasted; (ii) A cell that was subject to a critical deformation for a certain period of time τ^{th} does not re-enter the cell cycle again. (iii) If a critical deformation has lasted for a certain period of time τ^{th} the cell undergoes apoptosis (programmed cell death).
(VII) We model idealized situations with very fast or very slow lysis of dead cells by (i) removing or (ii) not removing dead cells.
We started our simulations for both the monolayer and the spheroids with one cell ($N(t = 0) = 1$). Since the initial cell population size $N(t = 0)$ in the experiments are not known, we shifted the curve along the t-axis until a good agreement between simulation results and experimental observations was obtained. The intersection of our computer simulation with the N-axis at $t = 0$ then permits to estimate $N(t = 0)$. (For the model parameters, see the table in appendix C.)

3. Results

3.1. Single-cell-based model

Figs. 3a,b show a typical time series of the tumor morphology and snapshots of the layer-like proliferation pattern in tumor spheroids for $N \geq 20000$ cells if dead cells are either not removed (a) or removed (b). The highest proliferation activity is close to the tumor boundary (in agreement with Ref. (Freyer, 1998, Bru et al., 2003)) where the local concentration of glucose is the highest, while inside the tumor a necrotic core forms. Although in monolayer cultures we assume no shortage of glucose (or oxygen), a characteristic proliferation pattern again forms above a certain population size (Figs. 3c,d). The corresponding simulated time developments of the tumor diameter and population size both show a good correspondence to the experimental findings for monolayers and tumor spheroids (Figs. 1a-d). As long as a tumor (cultured monolayer or tumor spheroid) is sufficiently small, the number of cells that have to rearrange if a cell in the tumor interior grows or divides is also small (even if cells form a dense aggregate or monolayer). Accordingly a growing cell in the tumor interior is in general able to exert a sufficiently strong force on its neighbors to push these aside or stimulate its neighbor

cells to migrate away. If at the same time each cell is supplied with glucose (and oxygen) then cells divide everywhere in the tumor hence the tumor grows exponentially fast (see Figs. 1b,d).

3.1.1. Tumor spheroids: In a tumor spheroid glucose and oxygen can enter the tumor only from its boundaries (Fig. 3a). The farther a cell is situated in the tumor interior the less glucose and oxygen are available because those cells which are closer to the boundary have already consumed much of the penetrating glucose and oxygen (Fig. 3a). As the tumor grows to a certain "crossover" size a layer-like structure is observed experimentally: a necrotic core is surrounded by a viable rim, that consists of an inner layer of quiescent cells and an outer layer of proliferating cells (Folkman and Hochberg, 1973, Sutherland, 1988). We denote this pattern as the "surface growth regime". In the surface growth regime the tumor diameter $L \approx vt$ (Fig. 1c). Since the experimental data also suggest $N^{1/3} \propto t$ (Fig. 1a), it follows $N \propto L^3$. I.e. the rescaled population size $N^{1/d} \approx \tilde{v}t$ also grows approximately linearly. While the growth velocity $v = dL/dt$ increases only by $\sim 7\%$ as the glucose medium concentration c_0 increases from $0.8mM$ to $16.5mM$ (Fig. 1c), $\tilde{v} \equiv d(N^{1/d})/dt$ increases by $\sim 65\%$. Hence for a given L, N increases with c_0. Now consider two cases: (a) In case the average cell size remains the same for all L, one obtains $N \propto L^3$ only if the total cell count includes the necrotic cells (debris). In this case $N \propto L^3$ denotes cells distributed over the tumor volume $V \approx (4/3)\pi(L/2)^3$. The relation between N and L would result from $N\overline{V}_c\varrho = V$ ($\overline{V}_c$ is the average cell volume, ϱ the cell density), i.e., the velocity of the spread v is proportional to $\tilde{v}$ if neither the cell density ϱ nor the average cell volume $\overline{V}_c$ change. However, in this case N is always the same for a given L, independent of c_0. That is, $N = fL^3$ where f is a constant independent of c_0 (as long as the cell size and density do not depend on c_0). Instead, $N = f(c_0)L^3$ is observed with $f(c_0)$ depending on c_0. If cells in the necrotic core were not included in the cell count, $N \propto L^2$ as long as neither the average cell size nor the average cell density change. This, however, is in contrast to the experimental observation. (b) For the simulated growth curves in Fig. 1a,c we removed the necrotic core and hence not did include it in the total cell count (Fig. 3b). Furthermore we modeled a decrease of the median cell volume with L (i.e., $\overline{V}_c \propto 1/L$) as observed by Freyer and Sutherland (1985) by the assumption that the daughter cells are slightly smaller than their mother cell (see assumption I(ii) for the explanation of this assumption). (Note, that if $\overline{V}_c \propto 1/L$, then $N \propto L^3$ and $L \propto t$ even if the viable cells N are confined to a surface layer of constant width.) The growth velocity $v \approx 2\Delta L/\tau_e$ increases with the effective thickness ΔL of the proliferating rim. τ_e is the effective cycle time and determined by the cycle time distribution (a detailed explanation of τ_e is given in section 3.2 and Fig. 7). $2\Delta L$ may be defined as the tumor diameter at the crossover between exponential and surface-growth regime, see below eqn (2). The small effect of c_0 on v suggests that c_0 has almost no effect on ΔL, in agreement with the conjecture by Mueller-Klieser (2000). Moreover, we eliminated the quiescence threshold from our simulation for $c_0 = 16mM$ (by setting $c_Q^{th} = c_{nec}^{th}$), and found v remains almost the

same. The explanation for this observation is that the quiescent cells that are mainly placed close to the necrotic core (Fig. 3a) are already under compression, and hence have a significantly larger than average cycle time such that they hardly contribute to the tumor expansion. Since most cell divisions occur close to the boundary, a quiescent threshold has to be sufficiently close to c_0 to influence ΔL significantly.
On the other hand we find the necrotic core at the same L is larger for smaller c_0 (the viable rim for $c_0 = 16mM$ was about $140\mu m$, for $c_0 = 0.8mM$ it was about $80\mu m$) hence c_0 in our simulations mainly controls N by the size of the necrotic core. To study which mechanism other than nutrient limitation may determine v, we studied $c_0 \to \infty$ (no nutrient limitation) and obtained a growth velocity v which is only $\sim 15\%$ above the value for $c_0 = 16mM$. We propose that v may largely be triggered by a biomechanical form of contact inhibition due to mechanical stress. In this case, the minor increase of v with c_0 may result from a small contribution of expansion forces from cells in larger viable rims for $c_0 = 16mM$ and for $c_0 \to \infty$.

3.1.2. Monolayer: The proposed form of contact inhibition would explain well the observed linear diameter growth in growing monolayers (Bru et al., 1998), in which all cells have access to nutrients (Fig. 1a,c; Fig. 3c,d). Our model predicts that, above a certain tumor size, cells sufficiently far in the tumor interior become jammed between so many surrounding cells that they are no longer capable of pushing their neighbors aside. This results in a large stress and a compression of cells inside the tumor which relaxes towards the outer boundaries where a small surface layer of cells is able to divide (Fig. 3c). Most cells that are affected by a growth stop (assumption VI) are situated in the interior and barely contribute to the expansion of the growing layer. Hence we found no difference in the expansion velocity whether or not interior cells were in principle able to re-enter the cell cycle (assumptions VI(i),(ii)). Even if the interior cells become apoptotic due to a too long lasting extensive stress (assumption VI(iii)) and are removed, v decreases only negligibly, since the space left by apoptotic cells is immediately refilled by dividing neighbor cells. Hence apoptosis does not affect the total cell number in our simulations. This explanation is supported by the observation of Bru et.al. (priv. comm., Bru et al. (2003)) that almost every cell was in close contact with its neighbors. The inherent coupling of mechanical stress and cell kinetics is also supported by the experiments in a series of papers by R.K. Jain and co-workers (e.g. Boucher et al. (1990), Boucher et al. (1997), Helmlinger et al. (1997)) and by Gutmann et al. (1992). Helmlinger et al. (1997), for example, have observed that with increasing relative amount of agarose in the growth medium the saturation size of expanding tumor spheroids decreases. With increasing agarose concentration the mechanical stiffness of the growth medium increases (see Fig. 9 for a computer simulation along this line). Alternatively, one may think of contact inhibition initiated by the interaction of cell surface receptor molecules. In this case, if cell-cell attraction is present, only the outermost cells of the monolayer would be able to divide, and the growth velocity would be $\sim 2l/\tau \approx 1\mu m/h$ (l: cell diameter), i.e. smaller than the value of $5.8\mu m/h$ found by Bru et. al. in Ref.

(Bru et al., 1998).
To explore the consequences of the suggested biomechanical form of contact inhibition in more depth, we predict the relaxation kinetics in case of total growth stop (Fig. 4), the growth kinetics at different biomechanical and migration cell parameters (Fig. 5 a-d); and the statistics of sub-clone sizes (Fig. 6). In case of a growth stop of all cells the cell population relaxes mechanical stress by expanding slightly (Fig. 4).
Our computer simulations suggest that an increase of (1.) the cell mobility (by increasing D, compare appendix A) or, analogously, a decrease of the friction between cells and their environment, or (2.) of the cells' (Young-) modulus E (the cell stiffness) delays the cross-over from exponential to linear growth of L and increases the monolayer growth velocity in the surface growth regime (Fig. 5a,b). A larger cell mobility or smaller cell-environment friction facilitate relaxation of the mechanical stress in the proliferating rim. However, migration over distances large compared to the cell diameter is not observed within the viable rim in our simulations. A larger E increases the force necessary to cause the critical cell deformation at which a stop of cell growth is triggered (model assumption (VI)). Hence both result in a larger size ΔL of the proliferating rim. Also a decrease of the critical deformation (or compression) threshold ζ (see assumption VI) reduces v (Fig. 5c,d). An inhibition of cell division triggered by a limitation of growth factors (e.g. Alberts et al. (2002)), for example, would not show the predicted behavior.
The sub-clone size is defined by enumerating all cells in chronological order from $k = 1, ..., N$ and counting the offspring $N_k(t)$ arising from cell $k(t)$ ($N_1 = N$ by definition). If each boundary cell at a given population size forms on average an equally large sub-clone, one would expect $\langle N_k \rangle = q(N-k)/N_p$ to hold for the sub-clone size averaged over many realizations of the stochastic growth process. Here N_p is the number of proliferating cells ($N_p = k$ in the exponential, $N_p = k^{d_s/d}\Delta L/l$, in the surface growth regime), q is a fit parameter, d_s is the global surface dimension, and d the dimension into which the tumor is expanding (for monolayers, $d_s = 1$, $d = 2$). The rescaling in Fig. 6b shows that the running average $\overline{N}_{k,\Delta k}$ (here over a window of size $\Delta k = 100$) can be well fitted by $\langle N \rangle$, i.e., $\overline{N}_{k,100} \approx \langle N \rangle$. For a larger thickness of the proliferating rim, and in exponentially fast growing monolayers where each cell has sufficient space to grow and divide, the fluctuations of the sub-clone sizes are small (Fig. 6a). However, the sub-clone size statistics show large fluctuations in the surface growth regime if the proliferative activity is concentrated at the monolayer boundary. While some cells form sub-clones of a much larger than average size, other cells that were born immediately before or after them may not have any offspring at all. The strong fluctuations may be explained by a competition of cells at the monolayer border for free space. Those cells that are at local convex positions of the border (see Fig. 3b) may either have a slightly smaller than average cycle time or have a slightly larger than average probability to reenter the proliferation cycle and therefore win the competition for free space against cells at local concave border positions. In some experimental settings, the cell substrate adhesion may not be strong enough to prevent some cells from losing contact with the substrate, and from being forced out of the monolayer by mechanical pressure. In this case the

expansion velocity may increase intermittently (Galle et al., 2005). For many cell lines, cells that loose substrate contact usually undergo apoptosis. Hence, mechanical stress would eventually again trigger a surface growth regime. In the case of purely active migration, the expansion velocity may be limited by re-organization processes within the cell, which then define a maximum migration velocity. However, note that the range of velocities found by Bru spans more than one order of magnitude (Bru et al., 2003). In the presence of cell-cell interaction, our qualitative results are very robust against changes of model details such as geometric details in the description of the cell division (Drasdo, 1996); of the form of contact inhibition; and of the detailed shape and strength of the interaction potential. In the absence of cell-cell adhesion, however, the initial tumor diameter grows as $L \propto t^\beta$ with $\beta \approx 0.5$, while the growth of N and the long term behavior again is the same as in the presence of cell-cell adhesion (Drasdo et al., 1995, Drasdo, 1996) This case is also qualitatively described by the Fisher-KPP-equation.

3.2. Phenomenological growth law

The inherent link between the generic growth kinetics and the morphology permits casting of the growth kinetics of a compact tumor in early expansion phases into a simple phenomenological growth law, in which cell population-specific behavior is subsumed in a small number of effective parameters. A phenomenological growth law can easily be handled by biologists and physicians and can be compared directly to their data. This is one reason why phenomenological growth laws enjoy wide interest. Based on our findings we suggest the use of L as characterizing quantity which can be fitted by

$$L(t) = L^{(0)}(t)H(t;t_{cr},n) + (1 - H(t;t_{cr},n))L^{(1)}(t). \qquad (2)$$

$H(t;t_{cr},n)$ is a step(-like) function and may be chosen as $H(t;t_{cr},n) = \frac{t_{cr}^n}{t^n+t_{cr}^n}$ (Hill function) with $n \gg 1$. t_{cr} is the crossover time from exponential to linear growth. $L^{(0)}(t) = L(t_0)exp\{t/(\tau_e d)\}$ describes the initial growth phase where $L(t_0)$ is the tumor size at $t = 0$. $L^{(1)}(t) = L^{(0)}(t = t_{cr}) + v(t - t_{cr})$ mimics the linear expansion phase with v being the expansion velocity. Since $H(t;t_{cr},n) \approx 1$ for $t \ll t_{cr}$, and $H(t;t_{cr},n) \approx 0$ for $t \gg t_{cr}$, eqn. (2) switches between the initial exponential growth phase to the linear expansion growth phase at $t = t_{cr}$. $\tau_e = \tau/\lambda$ is the effective cell cycle time observed in the exponential growth regime (Figs. 1b, 7a) and can be linked to the intrinsic cycle time τ by the cycle time distribution $f(\tau)$ as follows. $f(\tau)$ can be fitted by a Γ-distribution or by its discrete analog: an Erlang distribution $f(\tau') = \frac{n}{\overline{\tau}}\frac{(n\tau'/\overline{\tau})^{n-1}}{(n-1)!}e^{-n\tau'/\overline{\tau}}$ with $n > 0$ (Fig. 7). A population of non-interacting cells with this cycle time distribution can be shown to grow as $N \propto exp(\lambda t/\overline{\tau})$ with $\lambda \approx (2^{1/n} - 1)n \in [ln(2), 1]$. Note, that the intrinsic cycle time equals the average cycle time, $\tau \equiv \overline{\tau'} = \int_0^\infty \tau' f(\tau')d\tau'$ (compare Fig. 7). If excluded volume interactions do occur then some growth trials are rejected, the real average cycle time becomes $\overline{\tau}' \geq \tau$ and the cycle time distribution is no longer Γ-like (Fig. 7b). For a sufficiently peaked $f(\tau)$, $\lambda \approx ln(2)$. In the absence of resting, apoptotic, and necrotic cells within the proliferating rim, the thickness of the proliferating rim is given by $\Delta L \approx v\tau_e/2$. Hence, the crossover from exponential to linear growth is expected at

a tumor size of $L^{(0)}(t = t_{cr}) = 2\Delta L$ which yields an estimate for $t_{cr}(L(t_0), \tau_e, v)$ (Fig. 5a,b). The specific response of a compact growing cell population then is contained in the parameters $v = v(E, D, \zeta)$ and τ_e only.
Some experiments did show a saturation regime that follows the linear diameter growth (Folkman and Hochberg, 1973). Since no saturation was observed in our model, we conjecture that in the presence of nutrients in the growth medium, such a saturation regime must be the result of additional factors such as toxic chemicals secreted by necrotic cells (Freyer and Sutherland, 1986, Freyer, 1988).

4. Discussion

We present a model for the growth of tumor monolayers and tumor spheroids in vitro. Our model permits linkage of biomechanical and kinetic properties on the cellular and sub-cellular scale to macroscopic properties of multicellular aggregates, and the in-silico testing of hypotheses generated in experiments. Our computer simulations suggest that both the diameter and the population size N of compact tumors initially grows exponentially fast, but is followed by a linear expansion of the tumor diameter in monolayer cultures and in tumor spheroids. The comparison of our computer simulations to experimental findings (Freyer and Sutherland, 1985, 1986, Bru et al., 1998, 2003) suggests that the linear growth regime is characterized by a cell number increase confined to a surface layer. This may be triggered by mechanical stress in monolayers and to a large extent also in tumor spheroids. A nutrient limitation in tumor spheroids within the concentration ranges considered in this paper affects the expansion velocity only slightly and seems to determine mainly the cell population size by affecting the size of the necrotic core. In case the average cell size is approximately constant over the observation time, and in the absence of an apoptotic or necrotic core, the linear expansion regime is accompanied by a power law $N \propto t^d$. A linear increase of tumor diameter has also been observed in gliomas (Swanson et al., 2000), and can be found in tumor NIH3T3-Xenografts (which can be obtained from the data in Ref. (Schiffer et al., 2003) by rescaling) and in Glasgow osteosarcoma in mice (private communication from Elisabeth Filipski; the experimental data we used for the analysis were from the system described in Filipski et al. (2002)). This suggests that similar situations to those described in this paper also occur *in-vivo*. This, together with the remarkable robustness of our findings against changes of model details, suggest that the qualitative growth behavior at this stage is generic, while specific quantitative features (such as the crossover between the exponential and the linear expansion regime, or the expansion velocity) depend on cell-biomechanical or cell-kinetic parameters of the system under consideration. Accordingly we proposed a phenomenological growth law for the tumor diameter to which the data of initially expanding compact tumors can be fitted.
A number of predictions may be concluded from our model: (i) The cell cycle time of proliferating cells can be prolonged as a consequence of mechanical pressure on

the cell which, for sufficiently large cycle times, may even become apoptotic. This implies that cells at the tumor boundary have performed more cell divisions and accumulated many more mutations than cells in the interior, or in cells of a tumor of equal size that was generated by purely exponential growth (Fig. 8). (ii) If the proliferating rim is determined by the biomechanical form of contact inhibition, large sub-clone size fluctuations should occur if the proliferating rim is small (Fig. 6). This may be tested by clonal marker experiments in which, for example, individual cells at the tumor boundary are marked and the size of the sub-clones is measured after further growth. (iii) Above a certain glucose medium concentration the growth kinetics in tumor spheroids should become independent of the glucose medium concentration and determined by biomechanical interactions only. (iv) In case the degree of cell deformation (or compression) triggers the cessation of cell division, an increase of the cell "stiffness" or of the deformation (or compression) necessary to stop cell division should both result in an extended exponential growth regime, and in a larger asymptotic growth velocity in monolayer growth. This is no longer the case, if instead the cessation of cell division is triggered by a critical force threshold instead of a deformation threshold (Fig. 5). (v) An increase of the cell mobility or a reduction of the friction between cells and their environment should lead to an increase of the initial exponential growth regime and of the growth velocity in the linear regime. (vi) If cell division is repressed, the cells relax stress and the population slightly spreads. (vii) If cell/cell adhesion is absent, the population size initially grows exponentially fast while the aggregate diameter grows as $\propto \sqrt{t}$. The linear expansion regime remains.

Two possibilities for a careful validation of the predictions could be as follows. 1.) Experiments may be performed with different cell-lines under different growth conditions, where for each setting material quantities such as the elastic modulus (e.g. Alcaraz et al. (2003)), the strength of cell/cell-and cell/substrate-adhesion (Chesla et al., 1998, Zhang et al., 2004), the cell size, the proliferative activity (Gannon et al., 1998), apoptosis (Sayan et al., 2001, Schiffer et al., 2003), cell population size, tumor diameter, diffusion constant of cells (Mombach and Glazier, 1996), size of necrotic core (e.g. Freyer and Sutherland (1985)), and consumption rates etc. (Casciari et al., 1992)) would have to be measured. 2.) Alternatively, the kinetic or material properties of cells of one cell-line might be manipulated. However, since the manipulation of one cell parameter often results in changes of other cell parameters as well (e.g. Aplin et al. (1999)), a careful analysis of the cell and population parameters would again be necessary. A direct way to represent the effect of any kind of molecular modifications (as e.g. gene knockouts) on the multi-cellular phenotype would be to include an explicit representation of those elements of the intra-cellular molecular machinery that might be affected by the molecular modifications. This ensures that the effect of a molecular modification on all coarse-grained cell parameters is taken into account. In this way predictions of the multi-cellular behavior that result from molecular manipulations become feasible.

We do not claim that our model at its present stage is able to cover the whole potential

growth behavior that may occur in vitro. In our model of tumor spheroids we limited ourselves to the role of glucose. However, further factors can easily be included. One step may be to include an explicit representation of the ECM, in a first step for example as a random network of springs or visco-elastic elements that interact with the cells and locally control cell migration, division and apoptosis (Santini et al., 2000). However, as long as the cell density is large enough such that cells have close contact with their neighbor cells, this is not expected to modify the growth characteristics. On the other hand, if cells are loosely distributed in the ECM, such that they have no contact, the biomechanics of cell-cell interaction is not expected to determine the expansion of the tumor anymore. In this case, active migration as a consequence of, for example, cell-cell signaling together with the secretion of ECM-components by the cells may dominate the expansion velocity of the tumor. We also did not explicitly include the fluid pressure that may occur in the interior of the tumor spheroid and may thus contribute to the radial forces that leads to the tumor expansion. However, if the cells in the tumor are closely packed and adhere, this contribution should be small so that it can be neglected. A step towards the in-vivo situation may be to include tumor-environment interactions as observed in experiments by Helmlinger et al. (1997), or Koike et al. (2002). Fig. 9 shows a snapshot of a computer simulation along this line. Here a growing cell monolayer was enclosed by (non-proliferating) "cells" of another cell type B which mimics a visco-elastic medium. In this case, the monolayer size saturates. The larger the density of enclosing particles is, the smaller is the saturation size of the expanding monolayer (a detailed analysis is in progress). The smaller the deformation threshold ζ, the faster is the growth and an earlier the saturation occurs. Although in Fig. 9 we consider monolayers we expect the same qualitative behavior to hold for expanding spheroids as well as long as they are sufficiently small (as those in Ref. Helmlinger et al. (1997)). (Equivalent simulations with tumor spheroids are much more time-consuming.)

In conclusion we believe our model provides a useful framework for modeling the growth of cell populations in-silico. It may also be used as a guide in model building, for example, to set up appropriate rules of a CA, appropriate continuum equations, or to extract phenomenological growth laws (such as eqn. 2). The cell-biological and cell-kinetic parameters in our model were assumed to be the same for all cells and constant over time. Both assumptions are generally not true. Firstly, mutations can result in phenotypic changes that are reflected on the level of the coarse grained parameters (Gonzales-Garcia et al., 2002, Stein et al., 2004) Secondly, cells may actively control their biophysical and cell-kinetic properties (Santini et al., 2000, Huang and Ingber, 2000). However, both can easily be included into our model which then provides a link between the regulatory mechanisms on the molecular scale and the coarse grained bio-physical and cell-biological parameters (such as the elastic modulus, the Poisson number, the cell-cell (and cell-substrate) adhesion strength, and the cycle time) of the individual cell.

Finally, it should be noted that also spatio-temporal fluctuations, such as those which may occur if individual cells are killed in a stochastic process during chemotherapy or

radiation therapy of tumors, are naturally captured by our model approach (Santini et al., 1999).

5. Acknowledgements

The authors gratefully acknowledge helpful from discussions with A. Bru about monolayer growth, J.P. Freyer about expanding multi-cellular spheroids, J.G. Hengstler about Xenografts, and R. Kree about the sub-clone statistics, helpful hints to some references by J. Clairambault and J. Galle, and a critical reading of the manuscript by M. Cross, and a former manuscript version by H. Byrne, M. Lachmann and S. Ptak.

6. Glossary

Apoptosis: Programmed cell death of cells that commit suicide as a consequence of internal or external signals.

C6 rat astrocyte glioma cells: Animal neuroglial cell line of neuroepithelial origin.

Crossover Size (Point): Defined as the diameter (time) at which a tumor growth behavior crosses over from one growth regime to another growth regime. Within the paper we usually refer to the transition between exponential growth to surface-growth (where diameter grows linear in time).

EMT6/Ro-cells: Murine cell lines.

Intrinsic cycle time: Duration of the cell cycle of an average isolated cell not affected by physical interactions with neighboring cells. We assume an average intrinsic cell cycle time to be influenced at the level of individual cells by nutrients, regulatory factors and mechanical stress.

Linear velocity-force relationship: Velocity ($\underline{v}$) changes proportional to exerted force ($\underline{v} \propto \underline{F}$; $\underline{F}$: total force). This assumes that the migration velocity of a cell as a response on an external mechanical stimulus or force is approximately proportional to the strength of the stimulus. However, in case of a purely active migration process, reorganization processes within the cell are expected to eventually limit the migration velocity.

JKR Model: Johnson-Kendall-Roberts model for homogeneous elastic, adhesively interacting spherical bodies.

Spheroid: Tumor cells are often able to grow and divide anchorage-independent. I.e., they can be grown in suspension, not being attached to a substrate, where they form growing spherical aggregates (tumor spheroids).

Necrosis: Passive morphological changes that occur to cells of a tissue following their (non-apoptotic) death. Necrosis results from the cessation of energy-dependent processes that maintain the vital status quo.

Appendix A. Individual cell dynamics: Monte-Carlo-Method

Although growth is intrinsically a non-equilibrium problem we have modeled cell migration and growth by the standard Metropolis algorithm (Metropolis et al., 1953, Drasdo et al., 1995, Drasdo, 2000) which corresponds to the numerical integration of a master equation for the cell configuration. The use of this method is motivated by the observation that after each growth step all cells move to relax the configuration at least into a local equilibrium (Drasdo et al., 1995) (see also Fig. 4).

In the simulations, cells are randomly chosen from a "cell list" to perform a move trial. That is, either a small translation trial of step size ξ, orientation changes by rotations of the dumb-bell axis (in $d = 2$ around an angle of $\delta\alpha_j$, in $d = 3$ around the three space-fixed axes by an angle $\delta\alpha_j$ according to the algorithm of Barker and Watts, see Allen and Tildersley (1987)), or a growth trial of size δa. $\xi \in [0, \xi_{max}) \ll R$, $\delta\alpha_j \in [0, \delta\alpha_{max}) \ll \pi$ ($j = 1, 2, 3$ in $d = 3$ and $j = 1$ in $d = 2$) and $\delta a \in [0, \delta a_{max}) \ll R$ are uniformly distributed random variables. After the move trial the cell is removed from the cell list. This insures that each cell is touched exactly once at a given point of time, independently of the population size. When the list is empty, a new list with all cells that are present at this moment is generated and the time t increased by the period Δt. Between two successive growth trials a cell performs on the average $n_g \gg 1$ translation and rotation trials. Hence Δt is the time period between two migration or rotation trials. A cell not subject to any excluded volume interactions has an average cycle time $\tau \propto n_g$ (see appendix C). Each translation or rotation is accepted with probability $P_a = 1$ if $\Delta V^{tot} = V^{tot}_{t+\Delta t} - V^{tot}_t < 0$ and with probability $P_a = \exp(-\Delta V^{tot}/F_T)$ if $\Delta V^{tot} \geq 0$ (hence isolated cells move diffusively in accordance with Refs. (Schienbein et al., 1994, Mombach and Glazier, 1996)). F_T is an effective energy and may be viewed as a k_BT-analog to fluids or gases in cellular systems (T: temperature, k_B:Boltzmann const.) (Beysens et al., 2000) keeping in mind, however, that F_T is controlled by the cells and not the consequence of collisions with smaller particles. $V^{tot} = \sum_{i<j}^{N} V_{ij}$ summarizes the attractive and repulsive cell-cell interactions.

A growth trial is always accepted as long as it does not violate the condition $d_{ij} > \zeta(l_i - l_j)/2$ (apart from the simulations that lead to Figs. 5c,d, 9 we assumed $\zeta = 0.75$). This value corresponds approximately to the compression threshold (see below and Fig. 2).

Alternatively to the Monte Carlo approach, the cell dynamics may be modeled by stochastic equations of motion of the Langevin type for each individual cell where friction forces between a cell i and its environment (other cells $j \neq i$ and substrate) are balanced by the interaction forces $\sum_j \underline{F}_{ij} + \underline{F}_{is}$ with the neighbor cells j and the substrate s, and a white-noise stochastic force that models the active random cell movement (Dallon and Othmer, 2004, Galle et al., 2005). For example, in a homogeneous environment, the friction can be characterized by a coefficient γ and the diffusion by a diffusion constant D. The friction coefficient may be related to the parameter F_T and the diffusion constant according to $D = F_T/\gamma$ following the line of reasoning by Beysens et al. (2000). Cells

may migrate purely actively in response to an external mechanical stimulus. In this case, the "friction coefficient" subsumes the cell-internal reorganization processes, the protrusion of lamelipodia etc. during the cell migration process.

Appendix B. Interaction energy and force

With decreasing distance between the centers of the cells (*e.g.* upon compression), both their contact area and the number of adhesive contacts increase, resulting in an attractive interaction. On the other hand, if cells are spheroidal in isolation, a large contact area between them significantly stresses their cytoskeleton and membranes. Furthermore, experiments suggest that cells only have a small compressibility (the Poisson numbers are close to 0.5, Mahaffy et al. (2000), Alcaraz et al. (2003)). Both, the limited deformability and the limited compressibility give rise to a repulsive interaction. We model the combination of the repulsive and attractive energy contributions by the JKR-model (Carpick et al., 1999). This model is used to describe the interaction between two homogeneous elastic, isotropic, adhesive spheres. It assumes the spheres are able to deform as a consequence of adhesion. An important difference to the simpler Hertz model (Landau, 1975) is a hysteresis effect: when two spheres of radius R approach each other they spontaneously form a contact area of finite size at distance $d_{ij} = 2R$ while at $d_{ij} > 2R$ they had no contact (Fig. 2). When they are pulled apart they still have contact at distance $2R \leq d_{ij} \leq d_{ij}^c$. The force $F_{ij} \equiv |\underline{F}_{ij}(d_{ij})|$ (and the interaction energy V_{ij}) in the JKR-model can only be calculated numerically from the implicit equation (Carpick et al., 1999):

$$\delta = \frac{a^2}{\tilde{R}} - \left[2\pi\sigma a/\tilde{E}\right]^{1/2}, \tag{B.1}$$

where

$$a^3 = \frac{3\tilde{R}}{4\tilde{E}}\left[F_{ij} + 3\pi\sigma\tilde{R} + \left[6\pi\sigma\tilde{R}F_{ij} + (3\pi\sigma\tilde{R})^2)\right]^{1/2}\right]. \tag{B.2}$$

$\tilde{R}^{-1} = \frac{1}{R_i} + \frac{1}{R_j}$, and $d_{ij} = R_i + R_j - \delta$, $\tilde{E}^{-1} = \left(\frac{1-\nu_i^2}{E_i} + \frac{1-\nu_j^2}{E_j}\right)$, where E_i, E_j are the Young moduli, ν_i, ν_j the Poisson numbers of cells i and j, respectively. $R_i = l_i/2$ is the cell radius. δ denotes the central displacement and measures the deformation of two interacting cells along the axis that connects the centers of the nearest spheres of the neighboring dumb-bells i, j (Figs. B1, B2). $\sigma \approx \varrho_m W_s$, where ϱ_m is the density of surface adhesion molecules in the contact zone (Chesla et al., 1998, Piper et al., 1998) and W_s the binding energy of a single bond. The interaction energy V_{ij} has been obtained by numerical integration of the force $F_{ij}(d_{ij})$ using $F_{ij} = -|\underline{\nabla} V_{ij}|$. Both, the interaction force and the cell-cell interaction energy are shown in Fig. B2 in which further details are given.

For the tumor spheroid simulations in $d = 3$, we found a good agreement between the simulated and experimentally observed tumors for two situations: (i) if the cells maintain their radius R and the cell count N includes the necrotic cells. In this case,

however, it cannot be explained why N depends on c_0 for a given L, if at the same time the cell size and density within the tumor are the same for different c_0. (ii) if the necrotic cells are not included in N and a cell becomes smaller with each division according to $V \to 0.95V$ (with $V = 4/3\pi R^3$), hence $R = R(g)$ shrinks with the number of cell divisions g according to $R(g) = (0.95^{1/3})^g R$. I.e., $V_{ij} = V_{ij}(d_{ij}, R_i(g_i), R_j(g_j))$ for cells i, j which yields one curve for each (R_i, R_j). We emphasize that for the conclusions in this paper, it is the decrease of the average cell volume $\propto 1/L$ (as observed in Ref. Freyer and Sutherland (1985)) which is important rather than the mechanism responsible.

Appendix C. Parameters

In order to relate the numbers on the computer to physical quantities we introduce a length, a time and an energy scale and express all model parameters as multiples of these scales. As the time scale we introduce the average cycle time τ of an isolated cell, as the length scale we use the cell diameter at the beginning of the cell-cycle, $l = 2R$, and as the energy scale we used F_T ((Beysens et al., 2000), see above).

All other quantities are expressed in multiples of the reference scales τ, l, and F_T. (Since not all parameter values for the experimental settings in Refs. (Bru et al., 1998, Freyer and Sutherland, 1985, 1986) are known, we estimated their ranges from literature on similar systems.)

The model parameters not specified so far (the step sizes for migration, growth and the number of migration and rotation trials between two successive growth trials) are linked to literature parameters in the following way:

(1.) *time interval*:

$$\tau = \frac{n_g l(g)\Delta t}{\delta a_{max}(g)/2} = \frac{n_g l \Delta t}{\delta a_{max}/2} \Rightarrow \Delta\hat{t} \equiv \frac{\Delta t}{\tau} = \frac{\delta \hat{a}_{max}}{2n_g}. \tag{C.1}$$

(2.) *Diffusion constant*:

$$\hat{D} = \frac{\langle(\delta\underline{\hat{r}})^2\rangle}{2d\Delta\hat{t}} = \frac{(k\hat{\xi}^2_{max})}{(2d\Delta\hat{t})} \tag{C.2}$$

Here, $\hat{D} = D\tau/l^2$ is the dimensionless diffusion constant, $k = 2/5$ in $d = 3$, and $k = 1/2$ in $d = 2$. $l(g) = 2R(g)$. For shrinking cells in $d = 3$ we assume $\delta a_{max}(g) = (0.95^{1/3})^g \delta a_{max}$ to maintain the cell cycle time.

The parameters have been determined as follows.

(i) The diffusion constant D, the cell diameter l and the cycle time τ have been chosen (see table C1).

(ii) Eqn. (C.1) is inserted into eqn. (C.2).

(iii) The parameters $\delta\hat{a}_{max} \ll 1$ (≈ 0.02) and $n_g \gg 1$ are chosen, which, together with D, determine $\hat{\xi}^2_{max}$. $\hat{\xi}_{max}(\delta a_{max}, n_g, \hat{D})$ was chosen sufficiently small ($\ll 1$) in order to obtain a linear velocity-force relationship (i.e., increasing the applied force by a certain factor increases the migration velocity by the same factor). In case of purely active movement, the speed of the intracellular re-organization processes is expected to limit

$d=2$			
symbol	unit	value/range (used)	source
cell size l	μm	10	[1]
intrinsic cycle time τ	h	19	[1], [2]
Reference Energy F_T	J	$10^{-17} - 2\times10^{-15}$ (10^{-16})	[3], [4]
Young modulus E	Pa	$\sim 250 - 1000$ (270-900)	[5], [6]
Poisson number ν		$1/3 - 0.5$ (0.4,0.5)	[7], [8]
Cell diffusion const. D	cm^2/s	$4.7\times10^{-12} - 6.5\times10^{-11} cm^2/s$	[3]
Receptor surface density ϱ	m^{-2}	$\sim 10^{15}$	[9], [10]
Binding energy single bond		$\sim 25 k_B T$	[3]
τ^{th}/τ		$>\sim 2.5$	(assumed)
Maximum displacement ζ		0.75	
$d=3$			
cell size l	μm	$12 - 14.4$ (14)	[11], [12]
intrinsic cycle time τ	h	22	[12]
Reference Energy F_T	J	$10^{-17} - 2\times10^{-15}$ (10^{-16})	[3], [4]
Young modulus E	Pa	300-1000 (400)	[5], [6]
Poisson number ν		$1/3 - 0.5$ (0.4,0.5)	[7], [8]
Cell diffusion const. D	cm^2/s	2×10^{-12}	[3]
Gluc absorption rate $\hat{\gamma}$	$mg/(cell\, h)$	$7.5 - 21$ (7.5)	[13]
Receptor surface density ϱ	m^{-2}	$\sim 10^{15}$	[9], [10]
Binding energy single bond		$\sim 25 k_B T$	[3]
Necrosis threshold c^{th}_{nec}	mg/mm^3	6×10^{-6}	(assumed)
Quiescent threshold c^{th}_{Q}	mg/mm^3	2×10^{-5}	(assumed)
τ^{th}/τ		$>\sim 2.5$	(assumed)
Glc. diffusion const. D_{glc}	cm^2/s	$\sim 10^{-6}$	[14]
Maximum displacement ζ		0.6 - 0.81	

Table C1. [1]: Bru, priv. comm., [2]: DSMZ, [3]: Beysens et al. (2000), [4]: Schienbein et al. (1994), [5]: Davidson et al. (1995), [6]: Lekka et al. (1999), [7]: Mahaffy et al. (2000), [8]: Alcaraz et al. (2003), [9]: Chesla et al. (1998), [10]: Piper et al. (1998), [11]: Freyer and Sutherland (1985), [12]: Freyer and Sutherland (1986), [13]: Casciari et al. (1992), [14]: Casciari et al. (1988). The reference parameters with which we fitted the data by Bru et. al. (Bru et al., 1998) were $E_0 = 400Pa$ and $D_0 = 1.27\times10^{-11} cm^2/s$. We used $\nu = 0.5$ as in Ref. (Alcaraz et al., 2003). Note however, that different (ν, E) can result in the same interaction force F_{ij} since $\tilde{E}(\nu, E)$, not ν and E individually determine F_{ij} (e.g. for $\nu = 0.4, E = 450Pa$ the force is the same as for $\nu = 0.5, E = 400Pa$). For embryonic cells Beysens et. al. (Beysens et al., 2000) found $F_T \approx 2 - 8\times10^{-15} J$, experiments by Schienbein et. al. (Schienbein et al., 1994) with granulocytes suggest that $F_T =\sim 10^{-17} J$. Hence it is reasonable to assume that F_T may vary in the range of $10^{-17} J - 8\times10^{-15} J$ depending on the cell type and on the cell environment. We have chosen $F_T =\sim 10^{-16} J$.
The quiescence threshold c^{th}_{Q} has almost no influence on the simulation results. $0 < \zeta < 1$ quantifies how much a cells can be deformed in the presence of a load (see Fig. B1). $(1-\zeta)l$ determines how much a cell can be compressed in a certain direction. Apart from the simulations in Fig. 5c,d, we used $\zeta = 0.75$. If a cell remains un-deformed for a period of time larger than τ^{th} it stop proliferation (for a detailed explanation see model assumption VI(ii,iii)).

the migration velocity which we assume is not the case for the migration velocities considered here. Notice also, that the choice of $\delta\hat{a}_{max}$ and n_g, together with τ, also determines $\Delta\hat{t}$, which denotes the period of time between two successive move trials.

References

Mark S. Alber, Maria A. Kiskowski, James A. Glazier, and Yi Jiang. On cellular automaton approaches to modeling biological cells. In J. Rosenthal and D. S. Gilliam, editors, *Mathematical Systems Theory in Biology, Communication, and Finance*, pages 1–40. IMA 142, Springer-Verlag, New York, 2002.

B. Alberts, A. Johnson, J. Lewis, M. Raff, K. Roberts, and P. Walter. *The Cell*. Garland Science Publ., New York, 2002.

J. Alcaraz, L. Buscemi, M. Grabulosa, X. Trepat, B. Fabry, R. Farre, and D. Navajas. Microrheology of human lung epithelial cells measured by atomic force. *Biophys. J.*, 84:2071–2079, 2003.

M.P. Allen and D.J. Tildersley. *Computer Simulation of Liquids*. Oxford Science Publ., Oxford, 1987.

A.E. Aplin, A.K. Howe, and R.L. Juliano. Cell adhesion molecules, signal transduction and cell growth. *Curr. Op. Cell Biol.*, 11:737–744, 1999.

D. Beysens, G. Forgacs, and J.A. Glazier. Cell sorting is analogous to phase ordering in fluids. *Proc. Natl. Acad. Sci. USA*, 97(17):9467 – 9471, 2000.

Y. Boucher, L.T. Baxter, and R.K. Jain. Interstitial pressure gradients in tissue-isolated and subcutaneous tumors: implications for therapy. *Cancer Res.*, 50:4478–4484, 1990.

Y. Boucher, J. Salehi, B. Witwer, and R.K. Jain. Interstitial fluid pressure in intracranial tumors in patients and in rodents. *Br. J. Cancer*, 75:829–836, 1997.

A. Bru, J.M. Pastor, I. Fernaud, I. Bru, S. Melle, and C. Berenguer. Super-rough dynamics of tumor growth. *Phys. Rev. Lett.*, 81(18):4008–4011, 1998.

A. Bru, S. Albertos, J.L. Subiza, J.L. Garcia-Arsenio, and I. Bru. The universal dynamics of tumor growth. *Biophys. J.*, 85:2948 – 2961, 2003.

H. Byrne and L. Prezziosi. Modelling solid tumour growth using the theory of mixtures. *Mathem. Medicine and Biology*, 20:341 – 366, 2003.

H.M. Byrne, J.R. King, D.L.S. McElwain, and L. Preziosi. A two-phase model of solid tumor growth. *Appl. Math. Lett.*, pages 1–15, 2001.

R.W. Carpick, D. F. Ogletree, and M. Salmeron. A gerneral equation for fitting contact area and friction vs load measurements. *J. Colloid and Interface Sci*, 211:395–400, 1999.

J.J. Casciari, S.V. Sotirchos, and R.M. Sutherland. Glucose diffusivity in multicellular tumor spheroids. *Cancer Research*, 48:3905 – 3909, 1988.

J.J. Casciari, S.V. Sotirchos, and R.M. Sutherland. Variations in tumor cell growth rates and metabolism with oxygen concentration, glucose concentration, and extracellular ph. *J. Cell. Physiol.*, 151:386–394, 1992.

M.A.J. Chaplain. Avascular growth, angiogenesis and vascular growth in solid tumours: The mathematical modelling of the stages of tumour development. *Mathl. Comput. Modelling*, 23(6):47–87, 1996.

C.Y. Chen, H.M. Byrne, and J.R. King. The influence of growth-induced stress from the surrounding medium on the development of multicell spheroids. *J. Math. Biol.*, 43:191–220, 2001.

S.E. Chesla, P. Selvaraj, and C. Zhu. Measuring two-dimensional receptor-ligand binding kinetics by micropipette. *Biophys. J*, 75:1553–157, 1998.

J.C. Dallon and H.G. Othmer. How cellular movement determines the collective force generated by the dictyostelium discoideum slug. *J. theor. Biol.*, 231:203–222, 2004.

L.A. Davidson, M.A.R. Koehl, R Keller, and G.F. Oster. How do sea urchins invaginate? using bio-mechanics to distinguish between mechanisms of primary invagination. *Development*, 121:2005–2018, 1995.

D. Drasdo. Different growth regimes found in a monte-carlo model of growing tissue cell populations. In F. Schweitzer, editor, *Self organization of complex structures: From individual to collective dynamics*, pages 281–291. Gordon and Breach, 1996.

D. Drasdo. On selected individual-based approaches to the dynamics of multicellular systems. In J. Lenz W. Alt, M. Griebel, editor, *Multiscale modeling*. Birkhäuser, 2003.

D. Drasdo, R. Kree, and J.S. McCaskill. Monte-carlo approach to tissue-cell populations. *Phys. Rev. E*, 52(6):6635–6657, 1995.

Dirk Drasdo. Buckling instabilities in one-layered growing tissues. *Phys. Rev. Lett.*, 84 (18):4244–4247, 2000.

DSMZ. German collection of microorganism and cell cultures. *http://www.dsmz.de/*.

E. Filipski, V.M. King, X.M. Li, T.G. Granda, M-C Mormont, X.H. Liu, B. Blaustrat, M.H. Hastings, and F. Levi. Host circadian clock as a control point in tumor progression. *J. Natl. Cancer Inst.*, 94(9):690 – 697, 2002.

J. Folkman and M. Hochberg. Self-regulation of growth in three dimensions. *J. Exp. Med.*, 138:745–753, 1973.

J.P. Freyer. Role of necrosis in regulating the growth saturation of multicellular spheroids. *Cancer Research*, 48:2432 – 2439, 1988.

J.P. Freyer. Decreased mitochondrial function in quiescent cells isolated from multicellular tumor spheroids. *J. Cell. Physiol.*, 176:138–149, 1998.

J.P. Freyer and R.M. Sutherland. A reduction in the in situ rates of oxygen and glucose consumption of cells in emt6/ro spheroids during growthregulation of growth. *J. Cell. Physiol.*, 124:516–524, 1985.

J.P. Freyer and R.M. Sutherland. Regulation of growth saturation and development of necrosis in emt6/ro multicellular spheroids by the glucose and oxygene supply. *Cancer Res.*, 46:3504–3512, 1986.

J. Galle, M. Loeffler, and D. Drasdo. Modelling the effect of deregulated proliferation and apoptosis on the growth dynamics of epithelial cell populations in vitro. *Biophys. J.*, 88:62–75, 2005.

J.V. Gannon, A. Nebreda, N.M. Goodger, P.P. Morgan, and T. Hunt. A measure of the mitotic index: studies of the abundance and half-life of p34cdc2 in cultured cells and normal and neoplastic tissues. *Genes to Cells*, 3:17 – 27, 1998.

I. Gonzales-Garcia, R. Sole, and J. Costa. Metapopulation dynamics and spatial heterogeneity in cancer. *Proc. Natl. Acad. Sci. (USA)*, 99(20):13085 – 13089, 2002.

J. Guck, S. Schinkinger, B. Lincoln, F. Wottawah, S. Ebert, M. Romeyke, D. Lenz, H.M. Erickson, R. Ananthakrishnan, D. Mitchell, J. Käs, S. Ulvick, and C. Bilby. Optical deformability as an inherent cell marker for malignant transformation and metastatic competence. *Biophys. J.*, 88:3689–3698, 2005.

R. Gutmann, M. Leunig, J. Feyh, A.E. Goetz, K. Messmer, and E. Kastenbauer. Interstitial hypertension in head and neck tumors in patients: correlation with tumor size. *Cancer Res.*, 52:1993–1995, 1992.

D. Hart, E. Shochat, and Z. Agur. The growth law of primary breast cancer as inferred from mammography screening trials data. *Br. J. Cancer*, 78(3):382–387, 1998.

G. Helmlinger, P.A. Netti, H.C. Lichtenfeld, R.J. Melder, and R.K. Jain. Solid stress inhibits the growth of multicellular tumor spheroids. *Nature Biotechnology*, 15(8): 778–783, 1997.

S. Huang and D.E. Ingber. The structural and mechanical complexity of cell-growth control. *Nature Cell Biol.*, 1:E131–E138, 1999.

S. Huang and D.E. Ingber. Shape-dependent control of cell growth, differentiation, and apoptosis: Switching between attractors in cell regulatory networks. *Exp. Cell Res*, 261:91–103, 2000.

A.F. Jones, H.M. Byrne, J.S. Gibson, and J.W. Dold. A mathematical model of the stress induced during avascular tumour growth. *J. Math. Biol.*, 40:473–499, 2000.

C. Koike, T.D. McKee, A. Pluen, S. Ramanujan, K. Burton, L.L. Munn, Y. Boucher, and R.K. Jain. Solid stress facilitates spheroid formation: potential involvement of hyaluronan. *Brit. J. Cancer*, 86:947–953, 2002.

L.A. Kunz-Schughart. Multicellular tumor spheroids: intermediates between monolayer culture and in vivo tumor. *Cell Biology International*, 23(3):157 – 161, 1999.

D. Landau. *Theory of elasticity*. Pergamon, 1975.

M. Lekka, P. Laidler, D. Gil, J. Lekki, Z. Stachura, and A.Z. Hrynkiewicz. Elasticity of normal and cancerous human bladder cells studied by scanning force microscopy. *Eur. Biophys. J.*, 28:312–316, 1999.

R.E. Mahaffy, C.K. Shih, F.C. McKintosh, and J. Kaes. Scanning probe-based frequency-dependent microrheology of polymer gels and biological cells. *Phys. Rev. Lett.*, 85:880–883, 2000.

M. Marusic, Z. Bajzer, J.P. Freyer, and S. Vuk-Pavlovic. Analysis of growth of multicellular tumor spheroids by mathematical models. *Cell Prolif.*, 27:73–94, 1994.

N. Metropolis, A.W. Rosenbluth, M.N. Rosenbluth, A.H. Teller, and E. Teller. Equation of state calculations by fast computing machines. *J. Chem. Phys.*, 21:1087–1092, 1953.

J.C. Mombach and J.A. Glazier. Single cell motion in aggregates of embryonic cells. *Phys Rev Lett*, 76(16):3032–3035, 1996.

J. Moreira and A. Deutsch. Cellular automaton models of tumor development: A critical review. *Advances in Complex Systems*, 5(2-3):247–267, 2002.

W.J. Mueller-Klieser. Tumor biology and experimental therapeutics. *Critical Reviews in Oncology/Hematology*, 36:123–139, 2000.

M. Pfeiffer. Birds flock together. *Nature*, 395:324–326, 1998.

J.W. Piper, R.A. Swerlick, and C. Zhu. Determining force dependence of two-dimensional receptor-ligand binding affinity by centrifugation. *Biophys. J.*, 74:492–513, 1998.

J.P. Rivet and J.P. Boon. *Lattice Gas Hydrodynamics.* Cambridge Univ. Press, Cambridge, 2001.

P. Rosen and D.S. Misfeldt. Cell density determines epithelial migration in culture. *Proc. Natl. Acad. Sci.*, 77(8):4760–4763, 1980.

M.T. Santini and G. Rainaldi. Three-dimensional spheroid model in tumor biology. *Pathobiology*, 67:148–157, 1999.

M.T. Santini, G. Rainaldi, and P.L. Indovina. Multicellular tumour spheroids in radiation biology. *Int. J. Radiat. Biol.*, 75(7):787–799, 1999.

M.T. Santini, G. Rainaldi, and P.L. Indovina. Apoptosis, cell adhesion and the extracellular matrix in the three-dimensional growth of multicellular tumor spheroids. *Crit. Reviews in Oncology/Hematology*, 36:75–87, 2000.

B.S. Sayan, G. Ince, A.E. Sayan, and M. Ozturk. Napo as a novel apoptosis marker. *J. Cell Biol.*, 155:719–724, 2001.

M. Schienbein, K. Franke, and H. Gruler. Random walk and directed movement: comparison between inert particles and sel-organized molecular machines. *Phys. Rev. E*, 49(6):5462–5471, 1994.

I.B. Schiffer, S. Gebhard, C.K. Heimerdinger, A. Heling, J. Hast, U. Wollscheid, B. Seliger, B. Tanner, S. Gilbert, T. Beckers, S. Baasner, W. Brenner, C. Spangenberg, D. Prawitt, T. Trost, W.G. Schreiber, B. Zabel, M. Thelen, H.A. Lehr, F. Oesch, and J.G. Hengstler. Switching off her-2/neu in a tetracycline-controlled mouse tumor model leads to apoptosis and tumor-size-dependent remission. *Cancer Research*, 63: 7221–7231, 2003.

M. Seinberg. Reconstruction of tissues by dissociated cells. *Science*, 141:401–408, 1963.

W.D. Stein, T. Litman, T. Fojo, and S.E. Bates. A serial analysis of gene expression (sage) database analysis of chemosensibility: comparing solid tumors with cell lines and comparing solid tumros from different tissue origins. *Cancer Res.*, 64:2805 – 2815, 2004.

R.M. Sutherland. Cell and environment interactions in tumor microregions: The multicell spheroid model. *Science*, 240:177–184, 1988.

K.R. Swanson, E.C. Alvord, and J.D. Murray. quantitativ model for differential motility of gliomas in gey and white matter. *Cell Prolif.*, 33:317–329, 2000.

J.P. Ward and J.R. King. Mathematical modelling of avascular-tumor growth. *IMA Journal of Mathematics Applied in Medicine & Biology*, 14:39–69, 1997.

X. Zhang, A. Chen, D.D. Leon, H. Li, E. Noiri, V.T. Moy, and M.S. Goligorsky. Atomic force microscopy measurement of leukocyte-endothelial interaction. *Am J. Physiol. Heart Circ. Physiol.*, 286:H359–H367, 2004.

Figure Captions:

Fig.1: Tumor growth kinetics. (a): Scaled population size $N(t)^{1/d}$ vs. time t ($d = 3$ is the space dimension) for tumor spheroids. The symbols denote experiments by Freyer and Sutherland (1985, 1986) in a plot for different medium glucose (c_0) and oxygen (o_0) concentrations, the lines denote computer simulations to the data sets (2) (experiment: $\square$; computer simulation: dotted line) and (4) (experiment: $\blacksquare$; computer simulation: dashed-dotted lines). (1) c_0, o_0 ($\times$) not known (Freyer and Sutherland, 1985), (2) $c_0 = 16.5mM$, $o_0 = 0.28mM$, ($\square$) (3): $c_0 = 16.5mM$, $o_0 = 0.07mM$ (+), (4) $c_0 = 0.08mM$, $o_0 = 0.28mM$ ($\blacksquare$). The long dashed line denotes a simulation in $d = 3$ without nutrient limitation. (b): Initial growth of population size N in tumor spheroids for the data sets (2), (4) of (a) in a lin-log plot. The line denotes $N \propto e^{t/\tau_e}$ ($\tau_e \approx \tau/ln(2)$: effective cycle time, eqn. 2). (c): Plots of the tumor diameter L vs t for the tumor spheroid-data sets (2), (4) in (a), (b) and the corresponding simulations, and for the in-vitro monolayer growth data in Ref. (Bru et al., 1998) ($\bullet$). For tumor spheroids, in the linear regime we find $v = dL/dt = 71\mu m/d$ (no gluc limitation), $v = 61\mu m/d$ ($c_0 = 16.5mM$, $\square$), and $v = 56,5\mu m/d$ ($c_0 = 0.8mM$, $\blacksquare$). (d): lin-log plot for tumor spheroids. The full line denotes exponential growth.

Fig.2: (a) Illustration of the cell division algorithm. During cell division, a cell i deforms from a perfect sphere into a dumb-bell in small steps $\delta a \ll l_i$. l_i is the cell diameter of cell i immediately after division. (b) The cell-cell interaction energy V_{ij} vs. d_{ij}, the distance between the centers of the nearest spheres of the neighboring dumb-bells i, j in case the two cells with $l_i = l_j = l$ approach each other (full line, black arrows) or are pulled apart (red arrow). The shape of V_{ij} reflects the limited compressibility and deformability of the cells (Alcaraz et al., 2003), a hysteresis in case cells are pulled apart, and direct cell-cell adhesion (Chesla et al., 1998), (for details, see appendix B).

Fig.3: Simulated spatial growth patterns. (a), (b) denote tumor spheroids, (c), (d) monolayers. (a) Typical tumor growth scenario from $N(t = 0) = 100$ until $N = 200000$ cells in the last picture (shown for a three-dimensional spheroid). The arrows indicate the time direction. The colors in the upper right corner indicate different levels of the local glucose concentration, while the colors in the lower left corner indicate our classification of the cell state. Cells in the outer boundary layer (grey) form a proliferating rim enclosing a layer of quiescent (blue) cells and a necrotic core (black), where glucose has been depleted (red). In (a), necrotic cells are not removed from the tumor, in (b), they are removed. In (b), cells are assumed to shrink with increasing L (Freyer and Sutherland, 1985) (model assumption I(ii)). The size of the viable rim was approximately constant in time (Freyer and Sutherland, 1986). In monolayer cultures (c,d) almost all cells have a good access to glucose, but those in the interior (black) are not able to exert a sufficiently large force or stimulus on their neighbors to push them aside

and grow. In (c) we assumed these cells are not removed even if they eventually become apoptotic. Light cells denote the proliferative rim. The inset is a magnification of the boundary. The arrows in the inset indicate cells at positions of convex points of the surface which have a slightly shorter doubling time. (d) If cells that rest too long in a certain checkpoint of the cell cycle undergo apoptosis (the dark blue patches) and are removed quickly, surrounding cells re-enter the cell cycle and refill the empty space left by the apoptotic cells. In this case an irregular patch-like pattern that is formed in agreement with the observations of Bru (Bru, priv. comm.). In (a), (c), (d), $N \propto V \propto L^d$ hence if $L \propto t \Rightarrow N^{1/d} \propto t \Leftrightarrow N \propto t^d$ ($d = 2$ for monolayers, $d = 3$ for spheroids) as shown in Figs. 1a,b. In (b) $N \propto L^3$ is approximately maintained due to the shrinking of the median cell volume with increasing L. Within a proliferating rim the strongest proliferation activity was always found closest to the outer tumor boundary in agreement with Ref. (Bru et al., 2003).

Fig.4: (a) If the cell division is repressed the monolayer relaxes stress and slightly expands at constant cell number. The parameters are the same as for the monolayer simulation of the data of Bru (Bru et al., 1998) in Fig. 1c of the main text. $N = 10000$. (b) The relaxation of the diameter $L(t)$ (circles) follows the relation $A(1-exp(-Bt))+C$ (full line). Here A, B, C are fit parameters.

Fig.5: (a) Growth of monolayer diameter $L(t)$ (open symbols: simulations, closed circles: Bru data, see Fig. 1). An increase of the cell mobility (via D), or of the Young modulus E result in an increase of the expansion velocity $v = dL/dt$, and (b) extends the initial exponential growth regime. $E_0 = 400Pa$, $D_0 = 1.27 \times 10^{-11} cm^2/s$ is the reference data set for the simulations of Bru's data (also in Fig. 1). $90\mu m/d \leq v \leq 320\mu m/d$ is within the range observed for different cell lines in Ref. (Bru et al., 2003). The lines denote fits from eqn. (2) with $\lambda = 0.696$. In (a), (b), the symbols denote computer simulations, while in (c), (d) the black symbols and lines denote computer simulations. (c) Expansion for $0.6 \leq \zeta \leq 0.81$ (filled blue circles: Bru data, see Fig. 1). For larger ζ the growth velocity $v = dL/dt$ decreases since the cells stops growing at a smaller degree of deformation. At very small ζ, v does not decrease anymore as a consequence of a large cell compression. Note, however, that for too small ζ the linear theory is expected to fail, and moreover, the cell-cell pair-potential energy cannot be expected to yield a suffiently good approximation if a cell has more than one interaction partner. For the curves denoted by the star ("$*$") in (c) and (d), $E = 600Pa, \zeta = 0.81$. For the curves denoted by "+", $E = 600Pa$. For all other curves (squares, triangles right, triangles down), $E = 400Pa$. Our simulations further suggest, that if ζ for different E is chosen in such a way, that the force exerted is the same at the compression threshold, that is, $F(d_{ij} = 0.81l, E = 600) = F(d_{ij} = 0.75l, E = 400)$ (compare Fig. B2(a)), the corresponding expansion velocities are equal. A simple generalization of the model is to separate the critical deformation (or compression) at which a stop of growth is triggered from the maximal possible deformation (or compression) of the cell. We found, for ex-

ample, that if the growth stop is triggered at $d_{ij} = 0.81l$, while the minimal possible value for d_{ij} is at $d_{ij} = 0.75l$, we obtained a smaller expansion velocity than if both the growth threshold and the cell deformation (compression) threshold is at $d_{ij} = \zeta l = 0.81l$ (see the curve denoted by "+" in (c), (d)). (d) $dN^{1/2}/dt$ shows a monotonic increase with decreasing ζ.

Fig.6: (a) Sub-clone statistics N_k for the monolayers of Fig. 3d (red) and for the the parameters ($D = 5D_0$, $D = 0.37D_0$). For monolayer in the surface growth regime the running average $\overline{N}_{k,\Delta k}$, where Δk denotes the window size (here: $\Delta k = 100$) obeys the relation $\overline{N}_{k,\Delta k} \approx q_s(N-k)/(\sqrt{k}(\Delta L/l))$. This is illustrated in (b), in which we have drawn $Y \equiv \overline{N}_{k,100} \times (\Delta L/l)\sqrt{k}/(N-k) \sim q_s$ for $N = 10^5$ (details see text). The fluctuations of the sub-clone sizes are the larger the smaller are the proliferating rim or, equivalently, the smaller is the growth velocity v (τ is the same for all simulations). The decay of Y for $k <\sim 5000$ indicates the exponential growth regime.

Fig.7: (a) Cycle-time distribution for the cells in the exponential growth regime for expanding monolayers (histogram). The smooth curve denotes the Erlang-distribution with $m = 60$ and average $\overline{\tau'} \approx 0.785d$ (= intrinsic cycle time τ). $\lambda = 0.696$. (b) Cycle-time distribution for the cells in the surface-growth regime for expanding monolayers (histogram) and the parameters which were used to model the experimental data by Bru (Bru et al., 1998) (see table). The average of τ' is $\overline{\tau} \approx 1d > \tau$. The full curve denotes the Erlang-distribution from (a), the dashed curve an Erlang-distribution for $m = 15$. As the consequence of mechanical stress $\overline{\tau}$ increases, the cycle time distribution gets a (moderately) longer tail towards larger than the intrinsic cycle time. The distribution of cycle times τ' cannot be characterized by a Γ-like-distribution anymore.

Fig.8: Visualization of generation number for (a) D_0, E_0 and (b) $5D_0$, E_0 at $N = 10^4$ cells (compare also Fig. 5). Lighter colors denote larger generation numbers. The blue color denotes generation 15, i.e. all blue cells have performed 15 divisions. For the parameter setting in (a) the crossover size from exponential to linear expansion was at $N = 2000$ cells, for (b) at $N \approx 10^4$ cells. In the linear expansion regime, a clear radial generation pattern emerges where cells at the border have performed much more cell divisions than cells in the interior (a). In the exponential growth regime all cells have performed approximately the same number of divisions (b).

Fig.9: Monolayer cell population growing in an granular viscoelastic medium. (a) Morphometry. The cells of the expanding monolayer are white. The surrounding medium is modeled as elastic "cells" (yellow) that are incapable of growth and division and that do not adhere to each other or to the (white) cells. (b) Time series of robust diameter $L_{gyr} = 2\sqrt{2}R_{gyr}$ (L_{gyr} in μm), where $R_{gyr} = \sqrt{(1/N)\sum_{i=1}^{N}(\underline{r}_i - \overline{r})^2}$ is the radius of gyration for the monolayer, $\overline{r} = (1/N)\sum_{i=1}^{N}\underline{r}_i$ denotes its center of mass. If the monolayer

forms a perfect disc, $L_{gyr} = L$. While the expanding monolayer without any embedding visco-elastic medium does not stop expanding, the monolayer embedded in a cell-like medium does. The larger the initial density of cell-like-particles (= smaller initial distance) is, the smaller is the saturation size. The smaller the deformation threshold ζ is, the larger is the expansion velocity prior to saturation. Note the fast crossover to a linear expansion of L_{gyr}, as also observed by Helmlinger et al. (1997) for tumor spheroids in agarose gel.

Fig.B1: Two interacting neighbor cells i, j. The spheres illustrate the shapes of cells i, j if they were in isolation. The grey area denotes the shape of cell i interacting with cell j. δ_i is the central displacement which measures the deformation of cell i along the axis that connects cells i and j. The sum of insertions of both cells i and j is $\delta = \delta_i + \delta_j$.

Fig.B2: Cell-cell force $|\underline{F}_{ij}|$ (a) and cell-cell interaction energy V_{ij} (b) vs. distance d_{ij} in the JKR model (Carpick et al., 1999) for two cells of equal radius $R = l/2$ and different Young moduli. When cells approach each other (full line) they come into contact at $d_{ij} = 2R$ and immediately for a contact area. When cells are pulled apart, they loose contact at $d_{ij} = d_{ij}^c > 2R$ which reflects the hysteresis behavior. The larger the Young modulus E is, the larger is the force necessary to approach two interacting spheres (a). The cell-cell interaction energy is shown in (b). The full line at $d_{ij}/l \geq 1$ describes two cells that approach each other. The dashed curve in (b) has been obtained from the dashed curve in (a) by $V_{ij}^c = V^c(d_{ij}) = -\int_\infty^{d_{ij}} F(d'_{ij})d(d'_{ij})$ for $d_{ij} > \zeta(R_i + R_j)$. If two cells approach each other, $V_{ij} = 0$ if $d_{ij} > R_i + R_j$, $V_{ij} = V_{ij}^c$ if $\zeta(R_i + R_j) < d_{ij}/l < 1$, and ∞ otherwise. This construction insures, that $F_{ij} = -|\underline{\nabla} V_{ij}|$. Note that only the energy difference enters the MC-simulation. (However, in our simulations on cell growth the cells where always under compression.) At $d_{ij} = 0.75l$ which approximately corresponds to the distance that cells would have if they are densely packed such that they fill the whole space (with volume fraction ≈ 1) we assume a hard core repulsion. This takes into account that cells are almost incompressible with a Poisson number $\nu \approx 0.5$ (Alcaraz et al., 2003). A smaller distance would require cell compression.

Fig.1

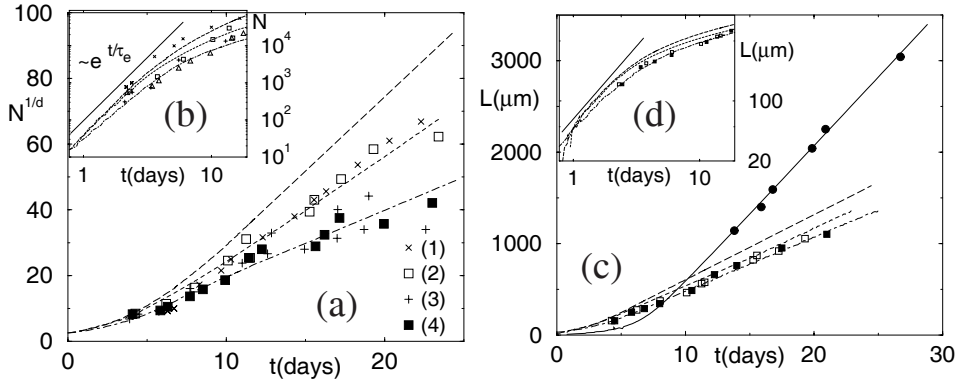
100
80
60
40
20
0
$N^{1/d}$
0
10
t(days)
20
(a)
(1)
(2)
(3)
(4)
$\sim e^{t/\tau_e}$
(b)
1
t(days)
10
N
10^4
10^3
10^2
10^1
3000
2000
1000
0
L(μm)
0
10
t(days)
20
30
(c)
(d)
1
t(days)
10
L(μm)
100
20

Fig.2

(a) 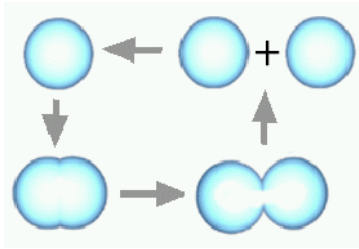

(b) 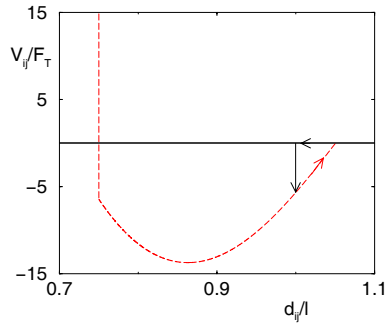

Fig.3

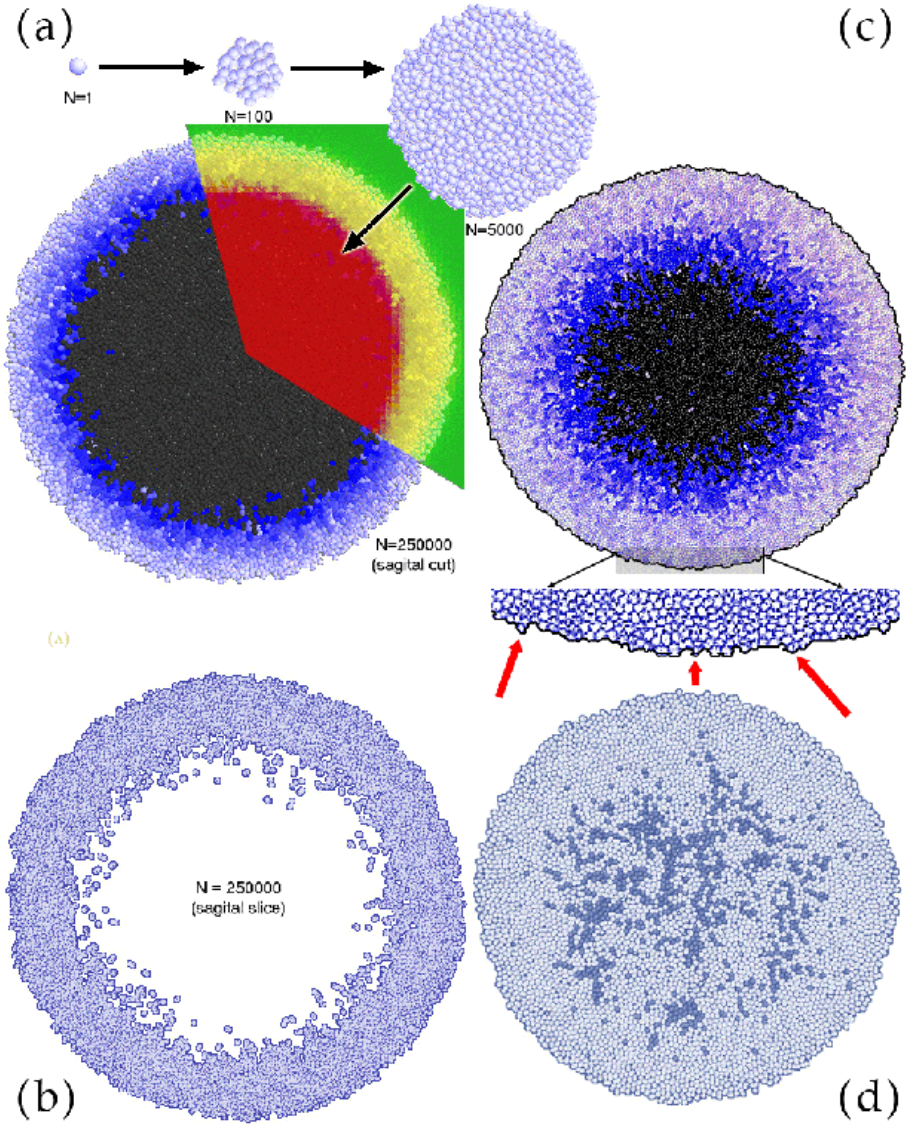
(a)
(c)
N=1
N=100
N=5000
N=250000
(sagital cut)
N = 250000
(sagital slice)
(b)
(d)

Fig.4

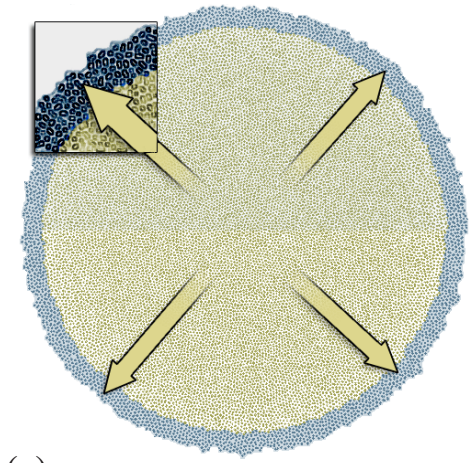

(a)

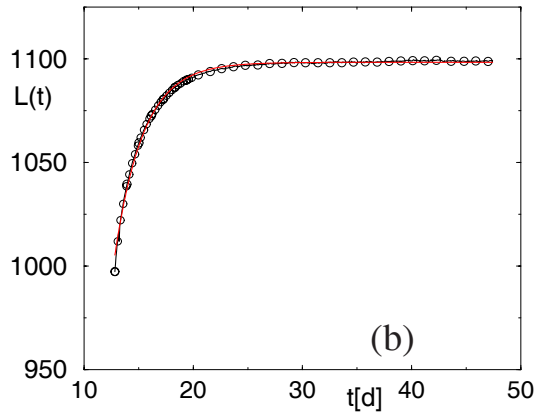

Fig.5

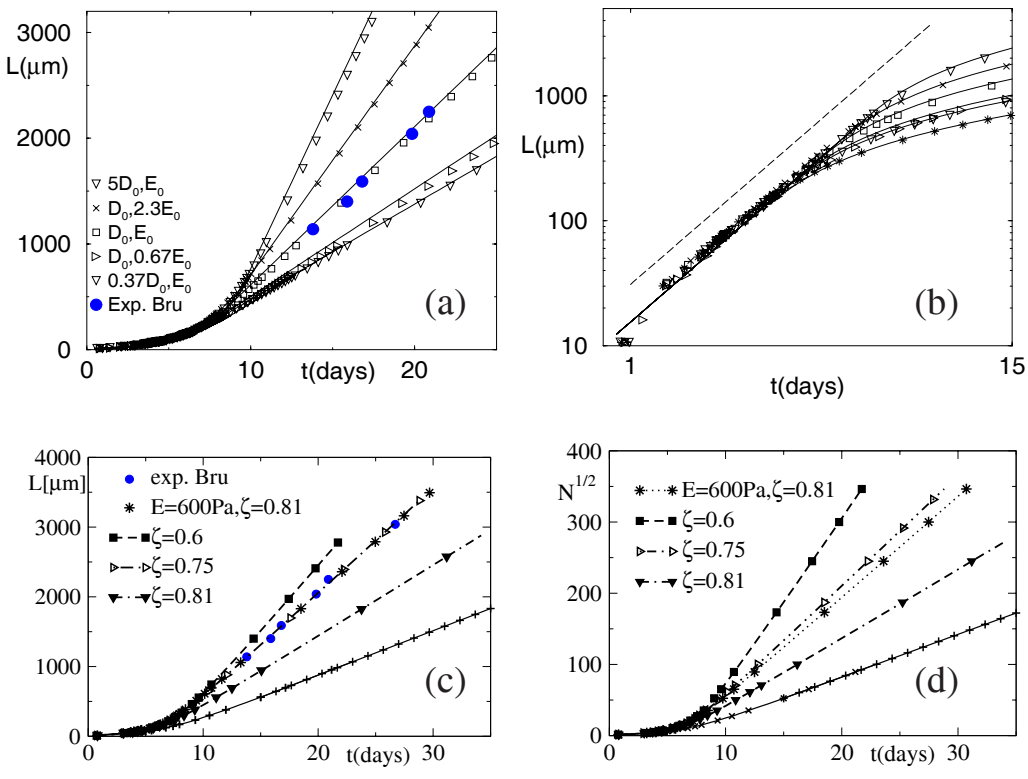
3000
L(μm)
2000
1000
0
0
10
t(days)
20
5D0,E0
D0,2.3E0
D0,E0
D0,0.67E0
0.37D0,E0
Exp. Bru
(a)
1000
L(μm)
100
10
1
15
t(days)
(b)
4000
L[μm]
3000
2000
1000
0
0
10
20
t(days)
30
exp. Bru
E=600Pa,ζ=0.81
ζ=0.6
ζ=0.75
ζ=0.81
(c)
400
N1/2
300
200
100
0
0
10
20
t(days)
30
E=600Pa,ζ=0.81
ζ=0.6
ζ=0.75
ζ=0.81
(d)

Fig.6

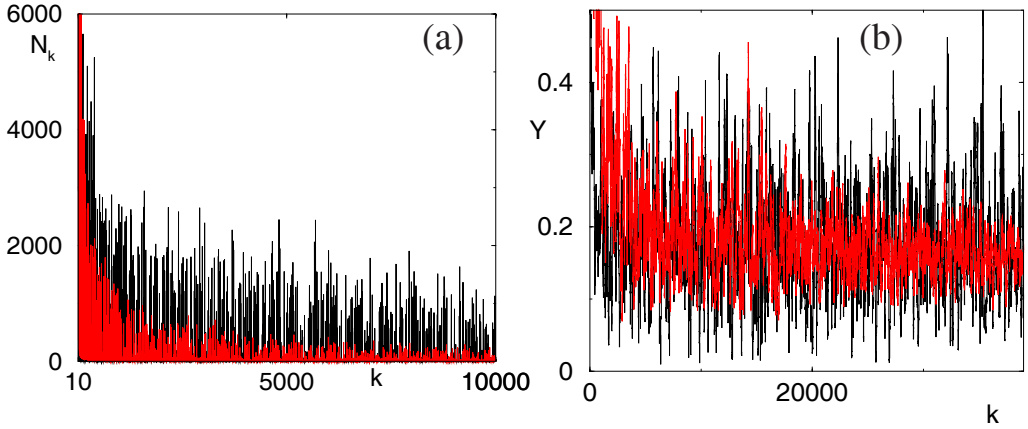

Fig.7

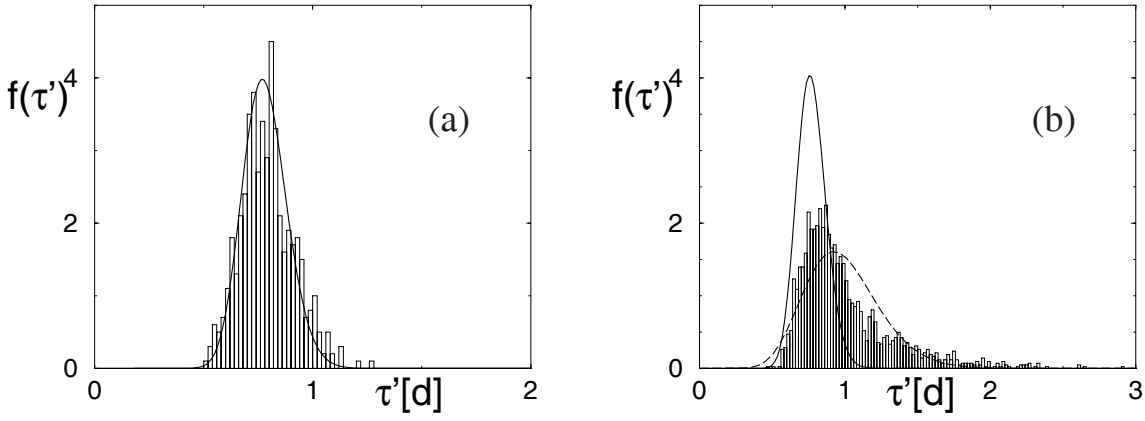

Fig.8

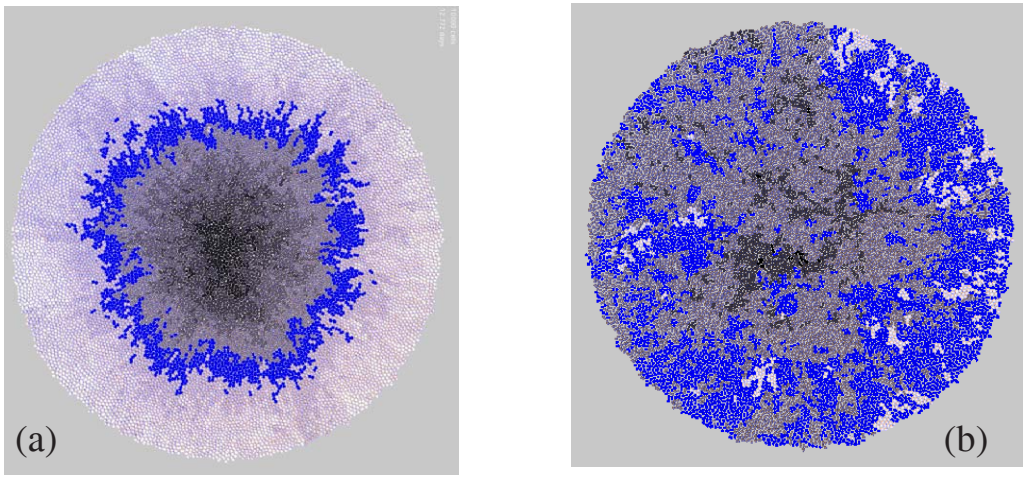

Fig.9

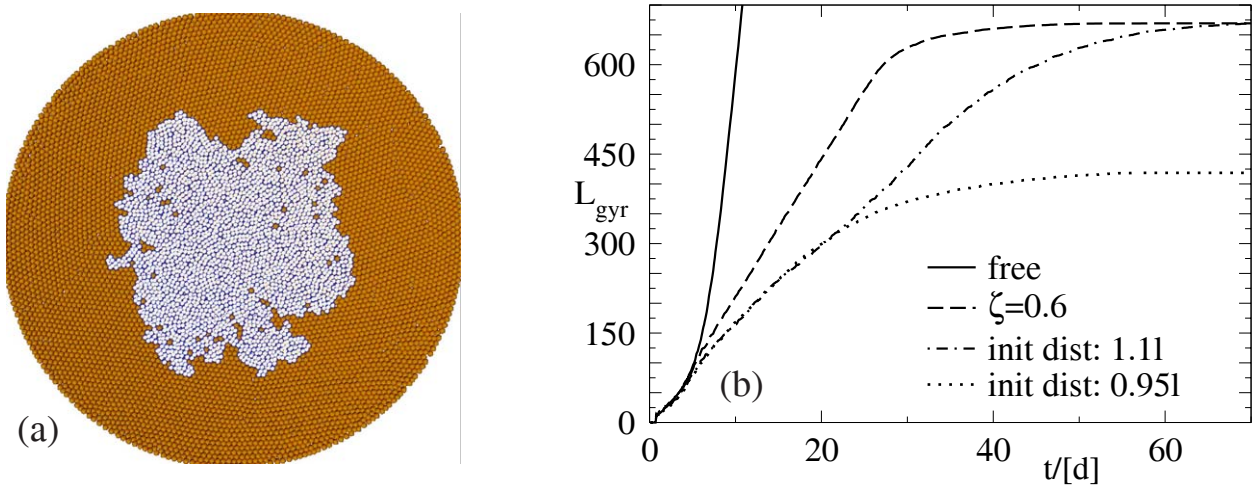
(a)
600
450
L_gyr
300
150
0
0
20
40
60
t/[d]
(b)
free
ζ=0.6
init dist: 1.1l
init dist: 0.95l

Fig.B1

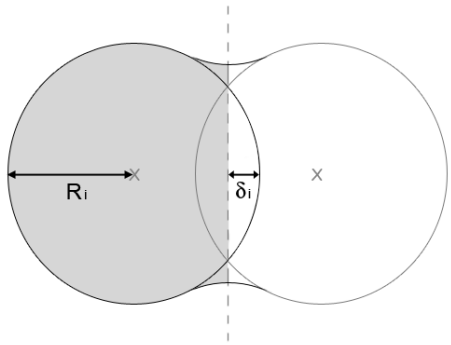

Fig.B2

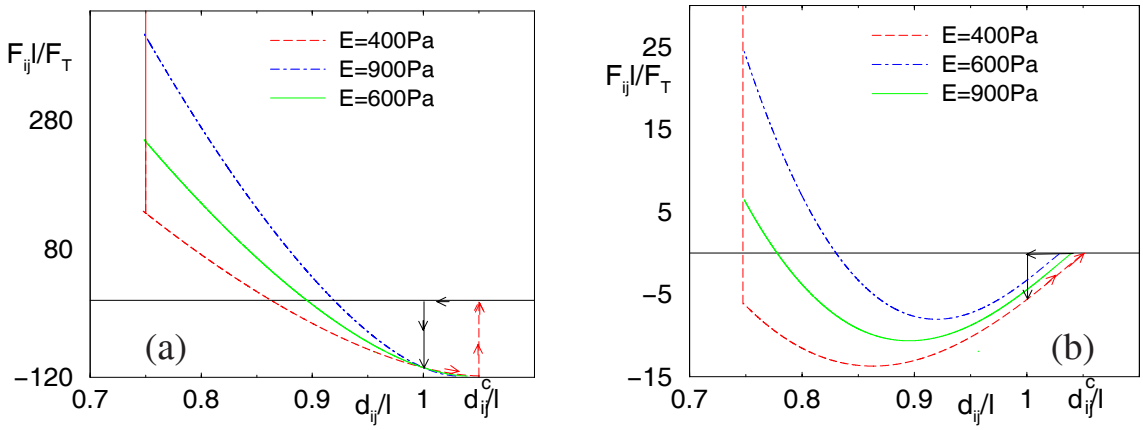
F_ij l/F_T
280
80
−120
0.7
0.8
0.9
d_ij/l
1
d_ij^c/l
E=400Pa
E=900Pa
E=600Pa
(a)
25
15
5
−5
−15
E=400Pa
E=600Pa
E=900Pa
(b)